The Susceptibility of Materials in Spallation Neutron Source Target and Blanket Cooling Loops to Corrosion

R. Scott Lillard, Darryl P. Butt

Materials Corrosion and Environmental Effects Lab
MST-6, Metallurgy Group
Los Alamos National Laboratory
Los Alamos, New Mexico 87545

Abstract

This paper presents our efforts and current progress in evaluating the susceptibility of materials in accelerator target / blanket cooling loops to corrosion. To simulate the environment that materials may be exposed to in a target / blanket cooling loop, samples were irradiated by an 800 MeV proton beam at the A6 Target Station of the Los Alamos Neutron Scattering Center (LANSCE). To accomplish this, a cooling water loop capable of exposing corrosion samples to an 800 MeV proton beam at currents upwards of 1 mA was constructed. This loop allowed control and evaluation hydrogen water chemistry, water conductivity, and solution pH. Specially designed ceramic / glass sealed samples were used to measure the real-time corrosion rates of materials placed directly in the proton beam using electrochemical impedance spectroscopy (EIS). EIS was also used to measure real-time corrosion rates of samples "down-stream" from the in-beam samples, out of the proton beam. These out-of-beam probes primarily examined the effects of long lived water radiolysis products from proton irradiation on corrosion rates. Weight loss samples in-beam and in high neutron flux areas were also used to evaluate corrosion rates. An overview of the LANSCE corrosion loop, the corrosion probes, and preliminary data from an in-beam Inconel 718 probe are presented. In addition, laboratory experiments demonstrating the effects of hydrogen peroxide (a water radiolysis product) on corrosion are also presented.

Introduction

Spallation neutron sources typically consist of a proton accelerator (Linac) and a shielded cavity which contains the neutron source (or target). This target is a high Z number metal, for example tungsten or tantalum, and in the case of tungsten may or may not be clad with a more corrosion resistant material such as Inconel. The proton beam leaves the high vacuum of the Linac via a "window" and enters the cavity were it strikes the target cavity. This window is typically constructed of Inconel and cooled by water. To keep the target cool (and to moderate the high energy neutrons which are produced) it is enclosed in a cooling loop which is generally constructed from stainless steel (SS304L) and filled with deionized water. This cooling loop may operate at upwards of 200 psi and flow rates on the order of 100's of gallons per minute. To produce tritium from a spallation neutron source, the cavity must also contain a set of blanket modules containing He^3 gas. These modules may be constructed from a number of materials such as aluminum alloys (Al5052, Al5053, Al6061), stainless steels (SS304, SS304L, SS316L-NUC), and lead. The blanket modules are also cooled by water, as may be the cavity itself. Thus, in the described spallation neutron source, components have the potential for failure due to pitting corrosion, crevice corrosion, stress corrosion cracking and galvanic corrosion.

In addition to the effects caused by aggressive halides, crevices, load, and dissimilar metals, the corrosion of materials in target / blanket cooling loops may also be effected by: 1) long lived water radiolysis products, 2) direct interaction between energetic particles and the material, 3) short lived water radiolysis products, or 4) some combination of each of these mechanisms. This paper will briefly review each of these mechanisms and present, in part, our experimental efforts at the Los Alamos Neutron Science Center (LANSCE) to measure the real time corrosion rates of materials in accelerator target / blanket cooling loops during irradiation. LANSCE provides the investigator with access to an 800 MeV proton beam. In this work, Electrochemical Impedance Spectroscopy was used to measure the real time corrosion rates of materials in the proton beam and down stream from the beam spot. To demonstrate the electrochemical effects of

radiolysis products on the corrosion rate of materials, a suite of laboratory experiments on tungsten is also presented.

Background

Effect of Proton Irradiation on Corrosion There have been very few studies on the corrosion behavior of materials in high energy particle beam environments. Simnad and Smoluchowski investigated the effects of a 260 MeV proton beam on the open circuit potential (OCP) of a tungsten target**[1]**. The sample was a 0.3 mm diameter wire which was annealed at 900^{o} C and degreased before being placed in the irradiation cell. Electrode potentials were measured during irradiation with respect to a saturated calomel cell by means of a vacuum tube potentiometer. The electrolyte was an oxygen-free, saturated KCl solution. They found for 260 MeV protons that the OCP of the tungsten sample became more positive at increasing proton fluences as shown in Table 1.

Their interpretation of this result was that the radiation field creates defects at the metal surface which contribute [somehow] to the observed electrode potential increase. They theorized that the defects had to be large (dislocation lines, loops, or collapsed vacancy clusters) because isolated vacancies and interstitials would presumably disappear rapidly given their proximity to the surface. In order to test the hypothesis that defects at the metal surface were responsible for the change in potential they took a fourth sample, irradiated it, then after the irradiation period annealed it at 900^{o} C. After the annealing period they measured the electrode potential of the W sample out-of-beam and found that it had returned to its original value. They concluded that the damage (and the corresponding enhanced corrosion) is reversible and can be "baked out". This assumes, however, that the interaction of the proton beam with the material produces a steady state condition which does not change once the sample is removed from the proton beam.

Table 1 Effect of 260 MeV protons on the open circuit potential of tungsten (from ref. **[1]**).

Sample Number	**Proton Fluence (p/cm^2)**	**Change in W Potential (mV)**

0	0	0
1	$1.8x10^{15}$	39
2	$6.8x10^{15}$	47
3	$2.2x10^{16}$	84

A similar study on the proton irradiation of iron**[2]**, addressed metal dissolution rates. The electrolyte was a pH 2, HCl solution. It was found for a fluence of $1x10^{16}$ p/cm^2 that the dissolution of the Fe_2O_3 layer at the surface of an iron electrode increased from 0.4 mg/cm^2 in the absence of irradiation to approximately 1.4 mg/cm^2 during irradiation.

Investigators have also evaluated the efficacy of corrosion inhibitors in particle accelerator cooling loops**[3]**. These studies have focused on the addition of hydrazine and benzotriazole at the CERN accelerator to mitigate copper corrosion in the magnet cooling water loops of the Linac. While water quality was improved by both inhibitors (evaluated by the concentration of Cu^{++} in solution), their use was limited to low radiation doses. Because of the high dose rates typical of a target blanket cooling loop these inhibitors are not likely to be acceptable.

Water Radiolysis Radiolysis models **[4,5,6]** have indicated that both oxidizing and reducing species are produced when water is irradiated with proton, neutron, or gamma radiation. These species are: H_2O, H_2, O_2, H_2O_2, OH, H, e^-_{aq}, HO_2, O_2^-, HO_2^-, OH^-, H^+. A list of some of the possible decomposition mechanisms for these species and their respective rate constants are presented in Table 2. As indicated by the reaction rate constants, the lifetime of many of these species is short, on the order of microseconds or less. While these short lived species may be an important consideration in the corrosion mechanism if they are formed at the metal / solution interface of the beam spot (i.e., the Helmholtz layer) they will have little impact on materials "down stream" in the cooling water loop.

Radiolysis products may also contribute to the corrosion reaction mechanism of “down stream” materials. The species which most influence down stream materials are hydrogen peroxide (H_2O_2) and oxygen (O_2), both of which are oxidizing species**[7]** and have lifetimes on the order of days or weeks. Oxidizing species are detrimental as corrosion reactions are generally

cathodically limited. That is, anodic and cathodic reactions at the rest potential are in equilibrium (i.e. you can not store charge) and the rate determining step is typically the cathodic reaction. Therefore, an increase in the concentration of an oxidizing species increases the rate determining step in the corrosion reaction and, correspondingly, increases the anodic (dissolution) reaction. As will be discussed later in this paper, experimentally the presence of H_2O_2 results in a positive shift in both the open circuit potential **[8]** and the corrosion current density **[9,10]**.

It may be possible to mitigate the formation of hydrogen peroxide in neutron spallation target cooling loops by using Hydrogen Water Chemistry (HWC) **[11,12,13,14]** similar to what is currently being used in commercial boiling water reactors. Hydrogen peroxide is formed from the chemical combination of two OH radicals produced during irradiation:

$$OH + OH \xrightarrow{k_{H_2O_2}} H_2O_2 \quad k_{H_2O_2} = 4x10^{9}\ (\text{mole sec})^{-1} \qquad \text{Eq. 1}$$

By bubbling H_2 gas into the cooling water the OH radical preferentially reacts with dissolved (atomic) hydrogen to form water according to the reaction:

$$OH + H \xrightarrow{k_{H_2O}} H_2O \quad k_{H_2O} = 2.4x10^{10}\ (\text{mole sec})^{-1} \qquad \text{Eq. 2}$$

While some valuable insight into the effects of radiolysis products on corrosion rates has been gained through laboratory simulation **[15]**, many of the radiolysis products are short lived and difficult or impossible to reproduce in the absence of a high energy radiation source. Therefore, a method for measuring the corrosion rates of materials in a prototypical cooling water loop is preferable. In this investigation the real-time corrosion rates of materials were measured during irradiation in and down stream from an 800 MeV proton beam. The focus of this investigation is to evaluate the roles of short lived radiolysis products, long lived radiolysis products, and direct proton beam / metal interaction on corrosion rate. In addition, a method for controlling HWC was employed.

Table 2 Elementary equations showing some of the water radiolysis products formed during irradiation, their decomposition mechanism, rate constant, and activation energy (from ref.**6**).

Reaction	**Rate Constant** (mole sec)$^{-1}$	**Activation Energy** (K cal/mol)

$e^- + H_2O = H + OH^-$	2.4×10^{10}	3
$e^- + OH = OH^-$	3.0×10^{10}	3
$H + H = H_2$	1×10^{10}	3
$e^- + HO_2 = HO_2^-$	2×10^{10}	3
$OH + OH = H_2O_2$	**4.5×10^{9}**	**3**
$H + OH = H_2O$	**2.4×10^{10}**	**3**
$H + O_2 = HO_2$	1×10^{9}	3
$OH^- + H_2O_2 = HO_2^- + H_2O$	1×10^{8}	4.5
$HO_2 = O_2^- + H^+$	8×10^{5}	3

I. Laboratory Experiments

I. A. Experimental

The W materials used in these experiments were 99.98% pure bcc electrodes mounted in epoxy. Prior to mounting, an electrical lead was connected to the back of each sample with silver paint. After mounting, the samples were polished with silicon carbide paper and finishing with successively finer grits of alumina on a polishing wheel. The final polish being 0.3×10^{-6} m alumina. Tungsten was chosen for these experiments as it is a target material and is currently in use at LANSCE as a spallation neutron source.

Test solutions consisted of deaerated 0.10 M NaCl with and without the addition of 10×10^{-3} M H_2O_2 (10 millimolar). The reference electrode used was saturated calomel (SCE). Potentiodynamic polarization curves were generated at a scan rate of 0.05 mv/s.

I. B. Results and Discussion

Potentiodynamic polarization curves for W in deaerated 0.10 M NaCl with and without the addition of 10×10^{-3} M H_2O_2 (10 millimolar) are presented in Figure 1. In these experiments the anodic portion of the polarization curves were generated with separate samples from those used to generate the cathodic portion of the curves (i.e., after the cathodic portion of the curve was generated, the sample was repolished and the anodic portion was then generated). As seen in Figure 1, the addition of H_2O_2 increases the open circuit potential (OCP) and the corrosion rate

(i_{corr}) but does not affect the anodic current densities. Further, for any given cathodic potential the cathodic current density is higher for the peroxide containing solution.

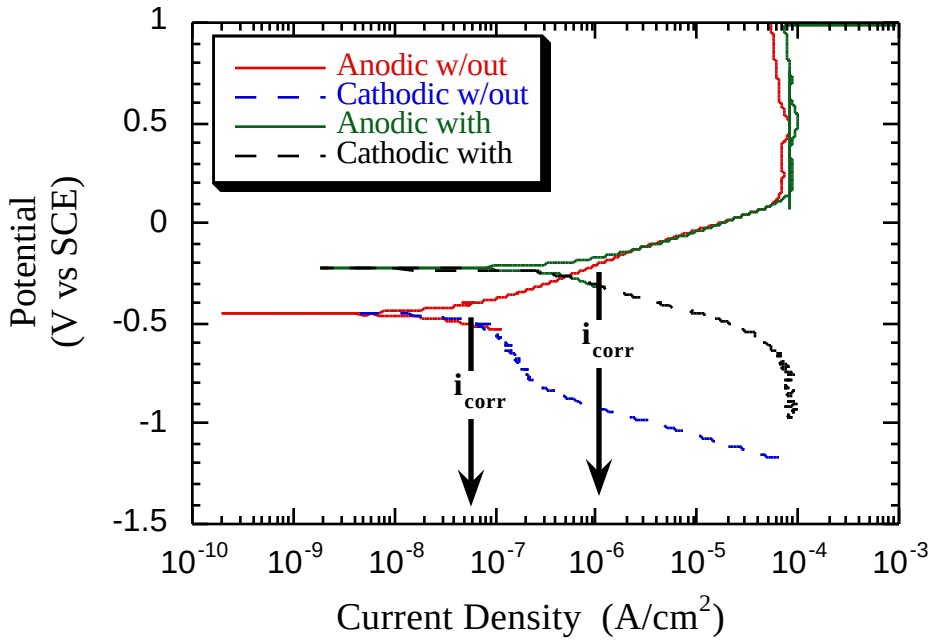

Figure 1 Anodic and cathodic potentiodynamic polarization curves for 99% tungsten in deaerated 0.1 M NaCl with / without 10 milliM of H_2O_2. Peroxide has no apparent effect on anodic dissolution rates, however, it markedly increases the cathodic reaction rate as seen by an increase in OCP.

The relevant thermodynamic equations which define the regions of stability and instability for H_2O_2 are**[16]**:

$2H_2O = H_2O_2 + 2H^+ + 2e^-$ $\quad E_o=1.78 - 0.059pH + 0.030\log(H_2O_2)$ Eq. 4

$2H_2O = HO_2^- + 3H^+ + 2e^-$ $\quad E_o=2.12 - 0.089pH + 0.030\log(HO_2^-)$ Eq. 5

$H_2O_2 = O_2 + 2H^+ + 2e^-$ $\quad E_o=0.68 - 0.059pH + 0.030\log(O_2/H_2O_2)$ Eq. 6

$HO_2^- = O_2 + H^+ + 2e^-$ $\quad E_o=0.68 - 0.089pH + 0.030\log(O_2/HO_2^-)$ Eq. 7

where HO_2^- is the peroxide anion, the concentration of O_2 is expressed in partial pressure, and potential is vs. normal hydrogen electrode. As shown in Figure 2, these relationships and their respective Nenrstian equations can be used to draw a diagram of electrochemical equilibria. At pH

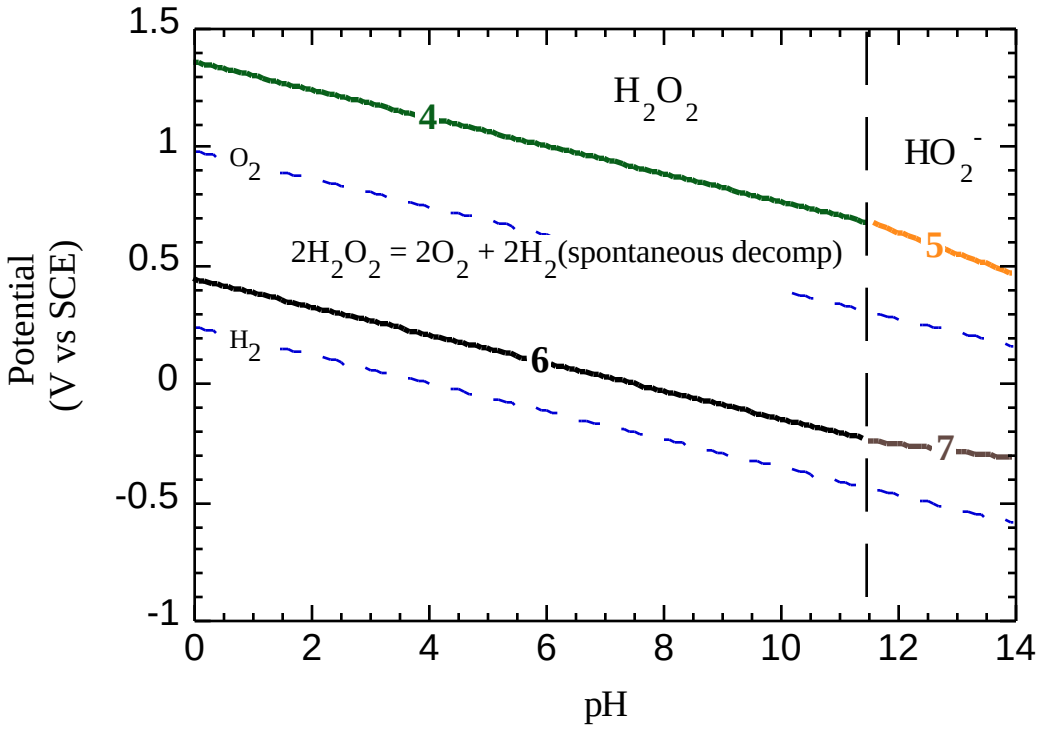

Figure 2 Diagram of electrochemical equilibria (Pourbaix diagram) for hydrogen peroxide in water. Numbered lines correspond to oxidation reactions Eq 4-7 above. This diagram was generated assuming $1x10^{-6}$ M H_2O_2 and HO_2^- and a H_2O_2/O_2 ratio equal to 1.

less than 11.6 and electrode potentials more positive than those defined by Equations 4 and 5, water is oxidized to form H_2O_2. At electrode potentials more negative than those defined by Equations 4 and 5, it will always be reduced to water. The domain defined by Equations 4-7 is a region of H_2O_2 chemical instability. In this domain, H_2O_2 may be electrochemically reduced or chemically decomposed (spontaneously) to water and oxygen:

$$2H_2O_2 = O_2 + 2H_2O \qquad \text{Eq. 8}$$

As seen in Figure 1 above, the OCP of W in deaerated 0.1M NaCl (pH 7) is approximately -0.50V SCE while the OCP of W in the same solution containing 10 milli-molar peroxide containing solution is approximately -0.25V SCE. From the Pourbaix diagram for hydrogen peroxide it is found that these potentials are in a region of peroxide reduction. Consequently, the primary role of H_2O_2 is as a cathodic reactant (i.e. Eq. 4 is controlling). Moreover, peroxide had

no effect on the anodic dissolution reaction as the anodic portion of each polarization curve in Figure 1 is identical. From these results we may conclude that hydrogen peroxide does not oxidize, reduce or chemically react with W-oxide as no change in the anodic half reaction was observed. It is also worth noting that if the OCP of the W was such that Equations 8 was controlling, the result would be the same as observed in the polarization curve because oxygen is also a cathodic reactant.

II. LANSCE Experiments

II.A. Design and Fabrication of the Corrosion Loop

The in-beam corrosion experiments in this investigation were carried out at the LANSCE A6 Target Station located in Experimental Area A just in front of the beam stop. A diagram of LANSCE is presented in Figure 3. While the A6 Target Station provides the investigator with a 1 mA, 800 MeV proton beam, it was necessary to design and fabricate a cooling water loop that would allow us access to it. A diagram representing the corrosion water system at the A6 Target Station is presented in Figure 4. This is a closed loop system filled with de-ionized water. The

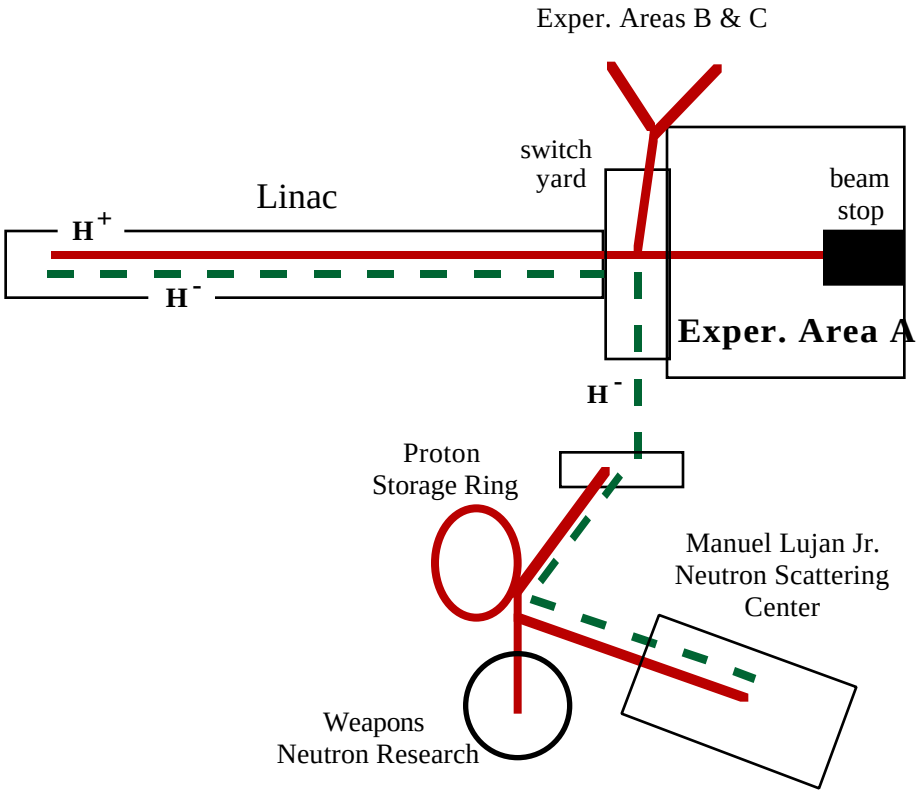

Figure 3 A diagram of the Los Alamos Neutron Scattering Center (LANSCE; not to scale, the Linac is approx. 1/2 mile long). The A6 Target Station is located in the Experimental Area A6 just in front of the beam stop.

pump nominally operates at 150 psi and a flow rate of 25 gal/min.

The out-of-beam corrosion probes are represented in Figure 4 as octagons marked "supply side" and "return side". These probes evaluate the effects of long lived radiolysis products and other solution contaminants on corrosion rate. The in-beam corrosion probes are represented by a rectangular box inside the dashed line that delineates the experiments at the base of the insert. These probes were placed directly in the proton beam and evaluate the effects of the proton beam interactions as well as short lived and long lived radiolysis products on the corrosion rates of

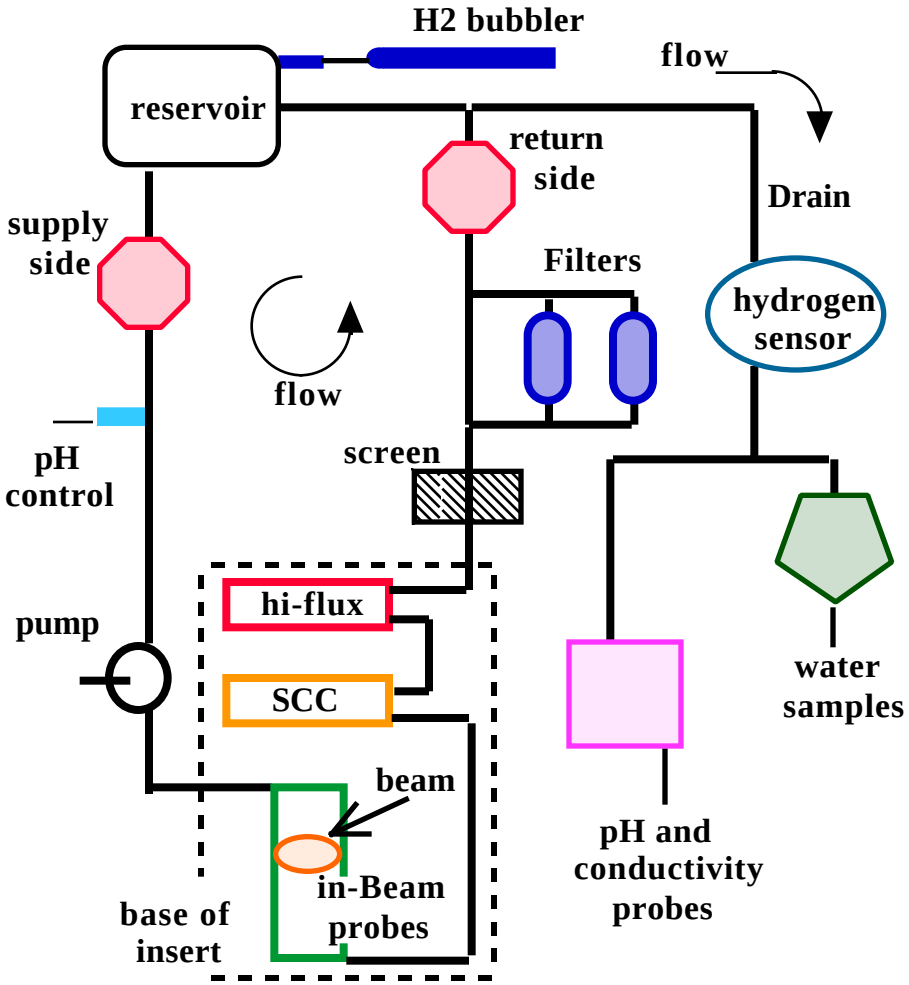

Figure 4 A diagram representing the corrosion diagnostics to be used on the cooling water loop at the LANSCE A6 target station. The proton beam is perpendicular to the diagram and is represented by the oval over top the in-beam corrosion probes

materials. Each of these probes and the remainder of the diagnostics presented in Figure 4 are detailed in the following sections of this paper.

In Beam Corrosion Probes One of the major goals of this program was the design and fabrication of corrosion probes to be used in-beam at the LANSCE A6 Target Station. To measure corrosion rate, it was necessary to electrically isolate the corrosion electrode from the cooling water loop. Conventionally, this can be accomplished with metal-to-glass seals. However, irradiation of the glass may cause it to become conductive, rendering the seal useless. Therefore, an alternate sealing method was chosen. As shown in Figure 5, the corrosion samples

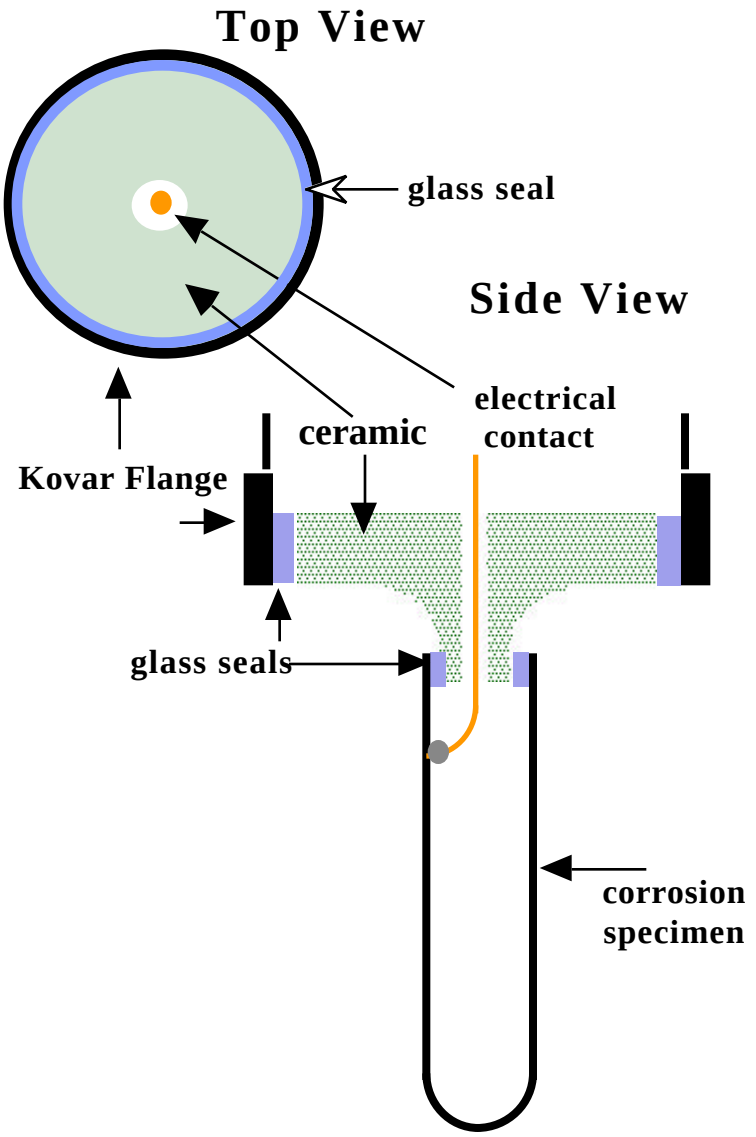

Figure 5 In beam corrosion probe to be used in the experimental corrosion water loop at the LANSCE A6 target station.

are cylinders (one end closed), 0.5" diameter x 6.25" length, that are joined to the ceramic by means of a compression seal. Because the corrosion samples have high expansion coefficients, the ceramic chosen for this application was alumina as opposed to Si_3N_4, for example, which may have been used if the corrosion samples had a low coefficient of thermal expansion. The temperatures required to form the compression seal (approximately 1000° C) ruled out the possibility of examining the corrosion rate of aluminum alloys in-beam. At the opposite end of the corrosion probe, the ceramic was joined to a Kovar flange by means of another compression seal.

This flange allowed the probe assembly to be welded to a SS304L water manifold. A diagram of the manifold is presented in Figure 6. This manifold consisted of 7 tubes arranged in a close packed array with tube #1 being in the front most position. The manifold was welded to the bottom of an 11' supporting insert in a manner to allow direct exposure of the samples to the proton beam. Each tube contained either an in-beam corrosion probe (Figure 5) or a weight loss foil (2" x 5/16" x 1/16") made from W, SS 304L, or Ta (noted as "**wl**" in Figure 6). Additional weight loss foils were placed down stream from the in-beam manifold in the high neutron flux area (Figure 4, "hi-flux"). While Electrochemical Impedance Spectroscopy was used to measure the real-time corrosion rate of the in-beam probes, weight loss requires samples to be weighed before and after exposure. From these measurements corrosion rate can be calculated from the expression:

$$CR = \frac{534\mathrm{m}}{\rho \mathrm{A} \mathrm{t}} \qquad \text{Eq. 3}$$

where **CR** is corrosion rate in mils/yr, **m** is weight loss (initial - final) in milligrams, ρ is density in grams/cm^3, **A** is the exposed surface area in in^2, and **t** is time of exposure in hrs.

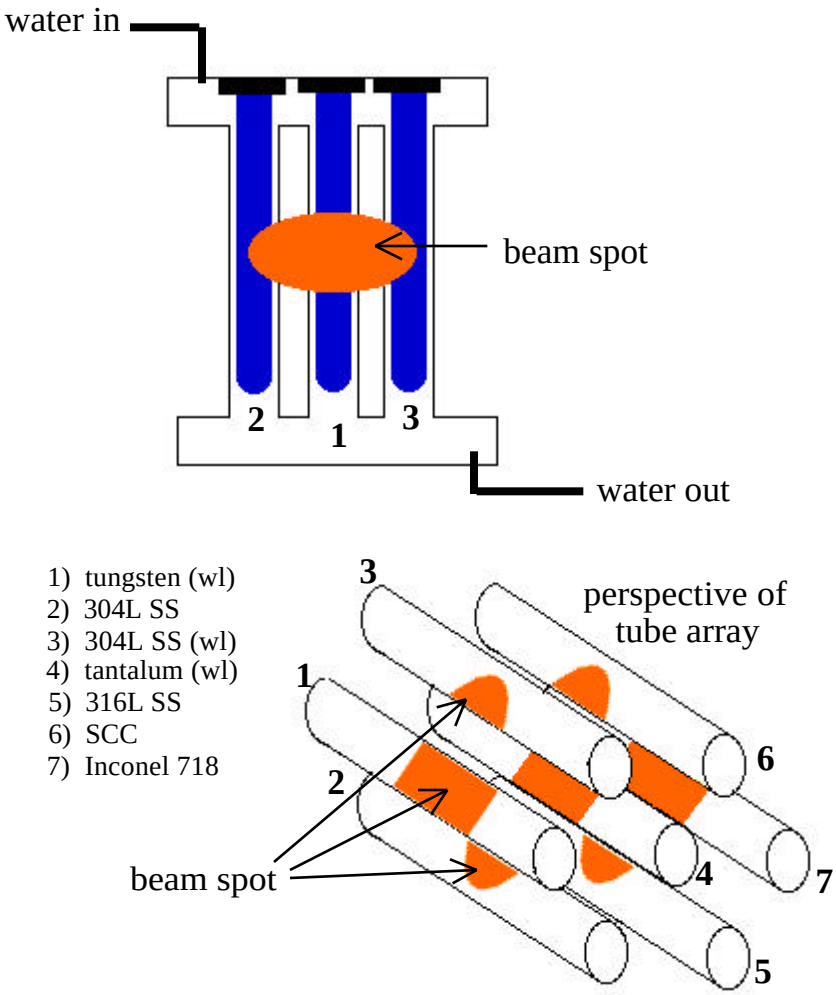

Figure 6 A diagram representing the placement of the in-beam corrosion probes in the manifold section the cooling water loop. This manifold is hung on an 11' steel insert to allow access to the beam at the LANSCE A6 target station. A list of the materials exposed to the proton beam and their position in the tube array is also presented, were the abbreviation 'wl' represents weight loss samples. All other samples are for measuring real time corrosion rates.

Out of Beam Corrosion Probes The corrosion probes used to measure out-of-beam corrosion rates at LANSCE were fabricated from commercially available NPT pipe plug style feed-throughs which electrically isolated the sample from ground via a glass seal. A diagram of this feed-through is presented in Figure 7. The samples were constructed from 0.125" diameter rods (up to 2" in length) of W, Ta, SS 304L, SS 316-NUC, IN718 , Al 5052, and Al 6061. These samples were seated onto studs which are sealed in glass. The pipe-plug assembly was fitted to one of 2 in-line corrosion cells (constructed from SS 304) on the cooling water loop at the top of

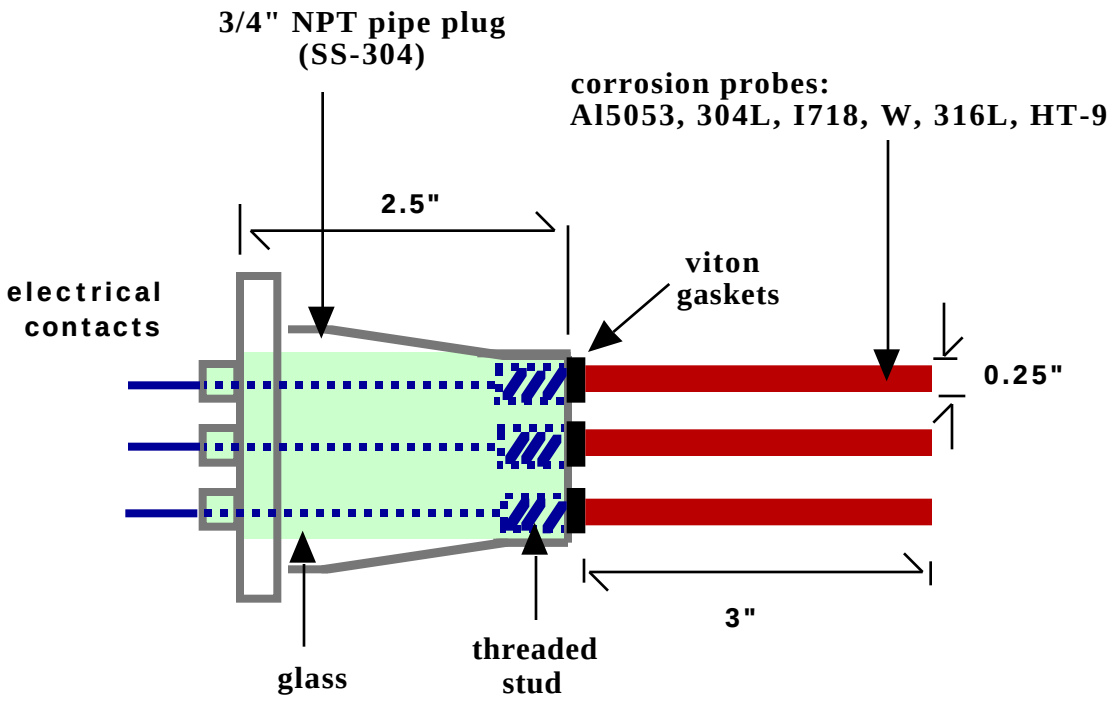

Figure 7 Out-of-beam corrosion probe to be used in spallation neutron cooling water loop at the LANSCE A6 target station.

the insert. Duplicate cells were placed on the supply side and the return side water lines which fed the in-beam probes (Figure 4; labeled "return-side" and "supply-side"). The corrosion rates measured by these probes are solely affected by changes in solution water chemistry such as the build up of hydrogen peroxide from water radiolysis or chlorides from improper cleaning.

Stress Corrosion Cracking Samples In an attempt to evaluate the combined effects of load and corrosion, stress corrosion cracking samples (designated as SCC in Figure 4) were also placed in the flow stream. They consisted of small u-bend specimens in accordance with ASTM standard G30-79**[17]**. These samples were placed below the insert to allow exposure to a combination of protons and a high flux of neutrons.

Water Chemistry Control and Evaluation In an attempt to mitigate the formation of hydrogen peroxide, hydrogen water chemistry (as is used in boiling water reactors) was implemented during the LANSCE irradiation experiments. This was accomplished by bubbling a

mixture of H_2 / 94% Ar gas directly into the water loop, ahead of the proton beam-spot. The dissolved hydrogen concentration in the cooling water loop during the LANSCE irradiation was monitored with a hydrogen sensor, Orbisphere Laboratories, Emerson NJ, (model #3610/220.E, TCD Hydrogen Gas System). Nominally, the system operated at a dissolved hydrogen concentration of 0.35 ppm. It has been shown for BWR / PWR reactors that the OCP is greatly suppressed during HWC**[9,11,18,,19,20,21,22,23,24]**. Moreover, as demonstrated in the previous sections of this report, hydrogen peroxide is a cathodic reactant. Therefore, minimizing its concentration should lower corrosion rates. It is for this reason that we feel HWC should be a key element to help minimize corrosion rates and extend material life-times in target / blanket cooling loops for accelerator spallation neutron sources. To evaluate the effect of hydrogen concentration on the real-time corrosion rates of in-beam and down stream samples, future work will include bubbling pure hydrogen into the system to maximize the dissolved concentration .

To monitor changes in water conductivity, probes were fabricated at LANL from the three-electrode out-of-beam corrosion probes shown in Figure 7 above. They were constructed by welding a hollow SS 304 sleeve onto two of the feed-through studs. This stainless steel sleeve (approximately 1.25" in diameter, 0.030" thick, and 3" long) surrounded a small stainless steel rod (also made from SS 304, approx. 0.125" thick and 2.5" long) which was welded onto the third feed through stud. This geometry allowed a probe cell constant (used to convert solution resistance to resistivity) to be determined more accurately than with the configuration used in earlier experiments on the LANSCE XO2 cooling water system**[25]**. Prior to placing these probes in the system, each was calibrated with solutions of known conductivity to determine its cell constant. Nominally the system operated at a water resistivity of approximately 0.07×10^6 ohm cm^2.

Additional water quality measurements were performed by Ion Coupled Plasma (ICP). By removing 100 mL aliquots of solution from the water system as a function of time and analyzing these samples for impurities, such as metal ion concentration, ICP allowed us to monitor the concentration of impurities (such as Cl^-) and corrosion products (such as W^{+6}) as a function of time.

II. B. Experimental Methods

The corrosion loop (discussed above) was fabricated entirely from SS 304. This includes all actuated and manual valves, filters, flow meters, pressure sensors, and pumps. Threaded parts were sealed with nuclear reactor grade pipe dope. While great care was taken to clean each individual part prior to assembly, after assembly the entire system was steam cleaned, rinsed with a mixture of ethanol and DI water (50/50) followed by 3 rinses with DI water. Once cleaned, the system was filled with DI water for operation.

Because the corrosion loop and future target / blanket cooling loops will use distilled and de-ionized water the initial solution resistivity in these systems will be on the order of 10^6 (ohm cm). In traditional dc electrochemical techniques for measuring corrosion rate, the solution resistance (R_{so}) can be neglected if it is small relative to the polarization resistance (R_p which is inversely proportional to corrosion rate); i.e. $V_{applied}/I_{meas} = R_{meas} = R_{so}+R_p$. Typical values for R_{so} are on the order 100 ohms or less as compared to R_p values generally on the order of 10^6 ohms. In deionized water, however, the solution resistance can be on the order of 10^5 ohms. Because this solution resistance is large, if not corrected for, the polarization resistance will be over estimated and as a result the corrosion rate will be underestimated.

Electrochemical Impedance Spectroscopy (EIS) is a powerful non-destructive technique for measuring the corrosion rates of metals in aqueous environments**[26,27,28]** and is ideally suited for systems with high solution resistivity. In EIS a small sinusoidal voltage perturbation (10 - 30 mV) is applied across the sample interface as a function of frequency. By measuring the transfer function of the applied ac voltage perturbation and the ac current response of the material, an impedance results ($Z\omega=V\omega/I\omega$). In the simplest sense, at low frequencies the material behaves as a resistor and $Z\omega=(R_{so}+R_p)$. At high frequencies, the material behaves as a capacitor and, therefore, offers no resistance to current. As a result $Z\omega=R_{so}$. By measuring $Z\omega$ over a wide frequency range the solution resistance can be determined and subtracted from the polarization resistance. Because the ac voltage perturbation used in EIS is small, it is a nondestructive

technique and corrosion rates can be measured at the material's "free corrosion potential" (i.e. its open circuit potential: OCP).

Because the stainless steel water system will act as an electrical sink for a traditionally grounded instrument, to use EIS as a tool for measuring corrosion rates a system isolated from ground (referred to as a "floating ground") was procured. With this system, a 2 electrode EIS measurement (working electrode / counter electrode) was used to measure the corrosion rate of the in-beam probes, while a conventional three electrode measurement (working / reference / counter electrodes) was used to measure the rates of the out-of-beam probes. The 2 electrode in-beam measurements were made possible by selecting a counter electrode with an effective resistance which was small relative to the polarization resistance of the corrosion probe. Here the stainless steel water system was selected as the counter electrode. Although the specific resistivity (polarization resistance) of the SS304 water system is on the order of 10^6 ohm cm^2, its area is large yielding an effective (measured) resistance of just a few ohms. Because it was possible to place several W/Woxide reference electrodes and C276 counter electrodes in proximity of the out-of-beam probes, the impedance of the counter electrode in the out-of-beam measurements was not an issue. It may also be noted that all EIS measurements were made at the OCP.

The materials examined at LANSCE were: Inconel 718 (IN718), low carbon stainless steel 304 (SS-304L) and nuclear grade 316 (SS-316L-NUC), aluminum alloys 5052 (Al5052) and 6061 (Al6061), 99.98% pure tungsten (W), 99.86% and pure tantalum (Ta). Ta and W were examined because they are target materials; the others are used in a variety of cladding and structure functions in the target / blanket cooling loop. Prior to placing the samples in the experimental irradiation loop, they were first abraded with 600 grit SiC paper, then degreased in acetone and ethanol then rinsed in deionized water. They were placed in the system after it was cleaned and prior to filling with deionized water

II. C. Preliminary Results and Discussion

Preliminary EIS data from the in-beam IN718 probe are presented in the form of Bode magnitude and phase plots in Figure 8. Inconel 718 is presented as it a crucial material, used to

construct the beam window between UHV and the target and cladding of W targets. The data in Figure 8 can be modeled as the electrical equivalent circuit presented in Figure 9. This circuit is known as a simplified Randles circuit **[29]**. By subtracting the solution resistance (R_{so}) from the low frequency impedance ($R_{so}+R_p$), the polarization resistance (R_p) for the Inconel 718 can be determined. This is most easily accomplished by using a complex non-linear least squares fit (CNLS) of the data and is shown in Figure 8. With the polarization resistance, corrosion rate can be determined from the well know expressions:

$$i_{corr} = 0.026 / R_p \qquad \text{Eq 9}$$

$$CR_{mpy} = \frac{129(i_{corr} EW)}{D} \qquad \text{Eq. 10}$$

where i_{corr} is the corrosion current density in milliamps/cm^2, R_p is the polarization resistance in ohm cm^2, EW is the equivalent weight in g/eq., D is density in g/cm^3, and CR is corrosion rate in mils/yr. The effect of beam current on the EIS response of the IN718 probe is presented in Figure 10. As can be seen in this plot as beam current increases, the low frequency impedance decreases. One of the goals of this research is to determine the corrosion rate of this material as a function of beam current and irradiation time from such plots so that a lifetime prediction for IN718 can be made.

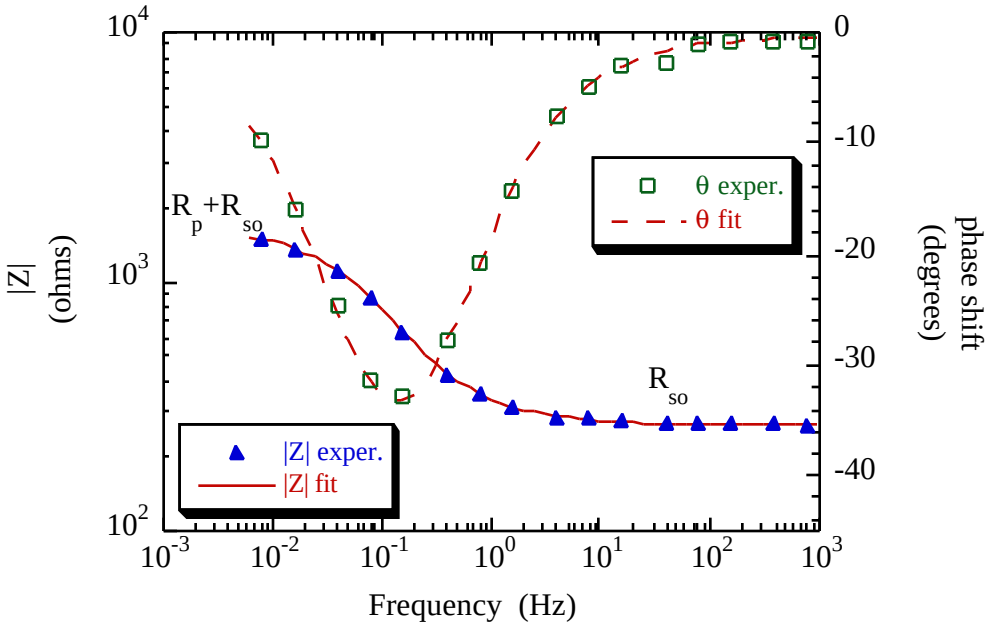

Figure 8 Bode magnitude and phase plots for the in-beam Inconel 718 probe during irradiation at a proton beam of 400μA. Data were taken during hydrogen water chemistry and at a temperature of approximately 60° C. (Note: only 30% of the experimental data are shown for clarity).

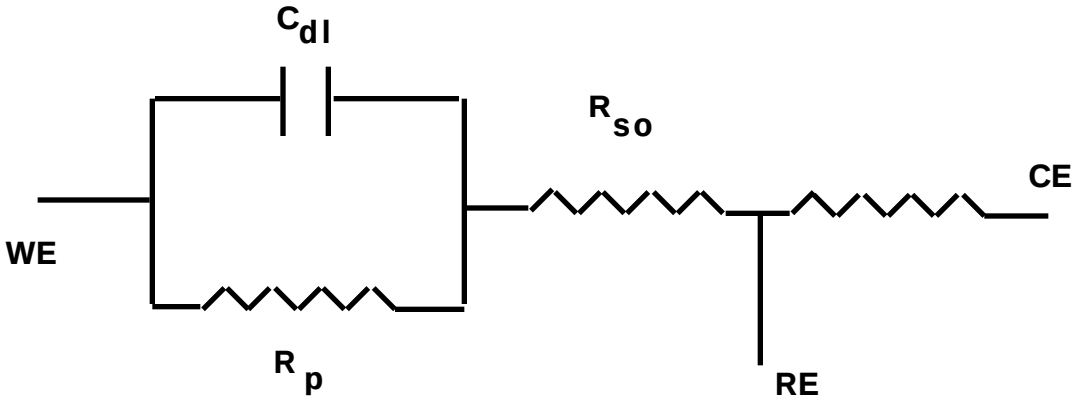

Figure 9 Simplified Randles circuit representing the electrical equivalent of the Bode magnitude and phase diagrams presented in Figure 8. Here C_{dl} represents the double layer capacitance, R_p represents the polarization resistance, and R_{so} represents the solution resistance. The symbols WE, RE, and CE represent the working, reference and counter electrode connections respectively.

For comparison, preliminary data from the out-of-beam IN718 probe (supply side) is presented in Figure 11. As can be seen in this Bode magnitude plot, the impedance at the low frequency limit ($R_{so}+R_p$) was not reached at the final measurement frequency of 0.005 Hz. However, there is sufficient data here to determine R_p from a CNLS fit of the data. From a qualitative comparison of this plot with the Bode magnitude data in Figures 8 and 10, it can be seen that the polarization resistance of the out-of-beam-probe is anticipated to be at least two orders of magnitude greater than the polarization resistance of the in-beam probe at the same proton beam current. While the out-of-beam probe measures only the effects of long lived water radiolysis products and solution contaminants on the corrosion rate of IN718, the corrosion rate of the in-beam probe is determined by these factors as well as direct interactions of the electrode surface and the proton beam. Direct exposure to the proton beam may increase corrosion rates (decrease R_p) due to production of short lived radiolysis products, high energy proton interaction with the metal/oxide, temperature increases, and changes in the electrochemical double layer.

In conclusion, the polarization resistance of in-beam IN718 probe has been found to decrease with increasing proton beam current. The polarization resistance of the out-of-beam IN718 probe was at least two orders of magnitude greater than that of the in beam probe.

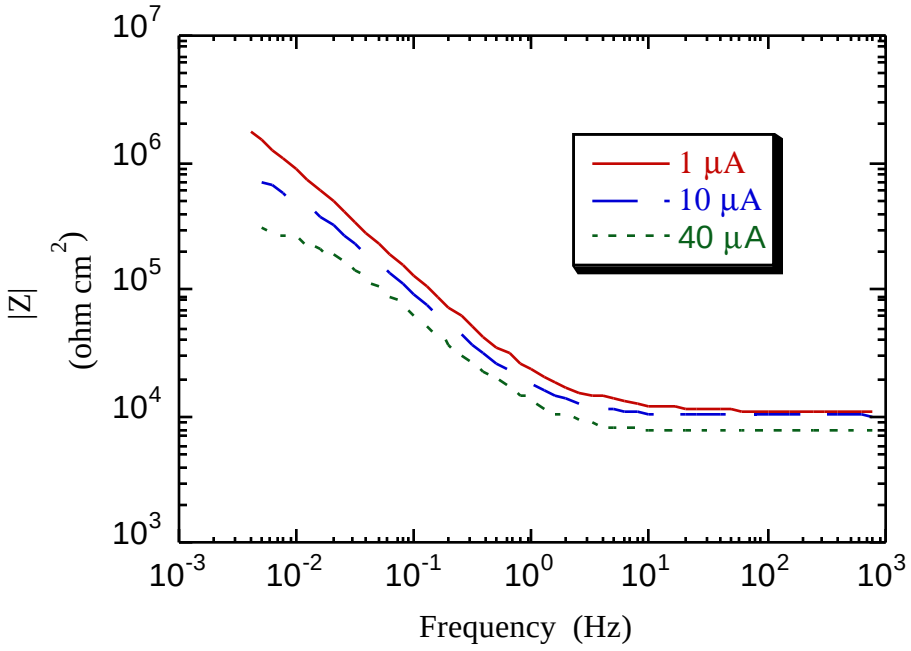

Figure 10 Bode magnitude plots for the I718 probe as a function of proton beam current. Data were taken during hydrogen water chemistry and with no other materials in front of the IN718 probe.

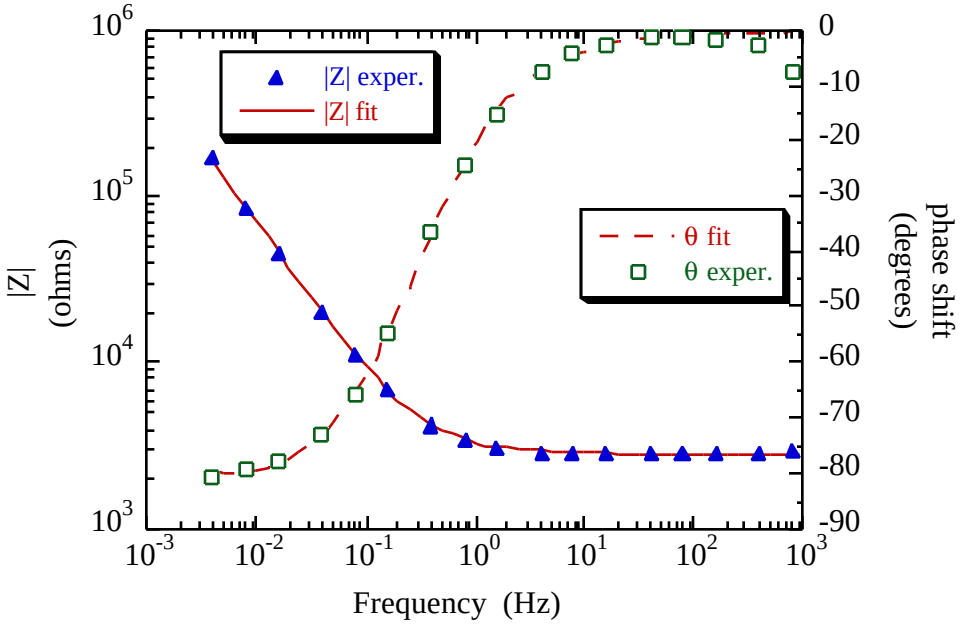

Figure 11 Bode magnitude plots for the IN718 probe as a function of proton beam current. Data were taken during hydrogen water chemistry and with no other materials in front of the I718 probe. (Note: only 30% of the experimental data are shown for clarity).

Summary

Laboratory experiments were conducted on tungsten electrodes to evaluate the effects of water radiolysis products on corrosion rate. In these experiments, potentiodynamic polarization curves for W were generated in 0.1M NaCl, with and without the addition of hydrogen peroxide. It was found that the primary role of H_2O_2 is as a cathodic reactant. Hydrogen peroxide has determined to have no effect on the anodic dissolution reaction or the oxide which forms on W.

A method for measuring the real-time electrochemical properties of materials used in spallation neutron source target / blanket cooling loops was also described. This test loop allowed the real-time corrosion rates of materials to be measured during irradiation in an 800 MeV proton beam at the Los Alamos Neutron Scattering Center has been described. This loop was equipped with in-beam corrosion probes, in-beam weight loss samples, out-of-beam corrosion probes and was also capable of controlling and evaluating hydrogen water chemistry, water conductivity, and solution pH.

To measure corrosion rate as a function of time, both in-beam and out-of-beam, it was necessary to electrically isolate the in-beam corrosion electrode from the cooling water loop. For the in-beam probes this was accomplished by means of a metal to ceramic seal. For the out-of-beam probes, samples were seated onto studs which were sealed in glass and joined to an NPT pipe plug style feed through. The pipe-plug assembly (which is commercially available) was fitted to an in-line corrosion cell on the cooling water loop at the top of the insert.

Preliminary EIS data from in-beam and out-of-beam IN718 corrosion probes were modeled as a simplified Randles equivalent circuit. From these experiments, it was demonstrated that the polarization resistance of the in-beam probe decreased with increasing proton beam current. Further, the polarization resistances measured on the out-of-beam probe were as much as 2 orders of magnitude greater than those measured on the in-beam probe at the same beam current.

At the end of the irradiation period (August 1997) a detailed analysis was begun of corrosion rate as a function of: proton beam current, irradiation time, and probe position (supply

side vs. return side) for all of the in-beam and out-of-beam probes. When this analysis is completed, an additional paper(s) will be submitted detailing these results.

Acknowledgments

All work on this project was completed under the auspices of the University of California for the US DOE contract #W-7405-ENG-36. The authors gratefully acknowledge: the support of Laurie Waters and the APT Project Office; the hands-on work of Donald Pile and Doris Ford; helpful discussion with Luke Daemen, Walt Sommer, Stuart Maloy, Gordon Willcutt, and the APT Materials Steering Committee; the engineering expertise of Richard Werbeck, Bob Brown and Eugene Zimmerman and countless others.

References

1 M.Simnad and R. Smoluchowski, **Physics Review**, vol.99 pp. 1891-2, 1955.

2 M.Simnad and R. Smoluchowski, **Physics Review**, vol.98, pp.1961-2, 1955.

3 F.E. Hoyer, "Radiolytic Corrosion in Cooling Water Circuits of High Energy Particle Accelerators and its Inhibition", in Proceedings, Fourth International Congress on Metallic Corrosion, N.E. Hamner ed., NACE, Houston, pp. 164-76, 1972.

4 J.L. Magee, A. Chatterjee, in Kinetics of Nonhomogeneous Processes, G.R. Freeman ed., John Wiley & Sons, New York, pp171-214, 1987.

5 H. Christensen, **Nuclear Technology**, vol. 109, pp. 373-82, 1994.

6 T.K. Yeh, D.D. Macdonald, A.T. Motta, **Nuclear Science and Engineering**, vol. 121, pp 468-82, 1995.

7 W.G. Burns, P.B. Moore, **Radiation Effects**, vol. 30, pp. 233-42, 1976.

8 R.S. Glass, G.E. Overturf, A. Van Konynenburrg, R.D. Mccright, **Corrosion Science**, vol. 26, no. 8., pp. 577-90, 1986.

9 H. Christensen, **Radiation Physical Chemistry**, vol 18, no. 1-2, pp.147-58, 1981.

10 W.G. Burns, W.R. Marsh, W.S. Walters, **Radiation Physical Chemistry**, vol. 21, no. 3, pp. 259-79, 1983.

11 M. Fox, "Water Chemistry and Corrosion in BWR's", *Corrosion/83,* paper no. 121, NACE, Houston, 1983.

12 M.E. Indig, J.E. Weber, **Corrosion**, vol. 41, no. 1, pp. 19-30, 1985.

13 J.J. Taylor, **EPRI Journal**, vol. 11, no. 3, pp. 54-55, 1986.

14 D.D. Macdonald, **Corrosion**, vol. 48, no. 3, pp.194-205, 1992.

15 D.D. Macdonald, H. Song, K. Makela, K. Yoshida, **Corrosion**, vol. 49, no. 1, pp. 8-16, 1993.

16 M.Pourbaix, Atlas of Electrochemical Equilibria, NACE, 1974.

17 Annual Book of ASTM Standards, 03.02, Wear and Errosion; Metallic Corrosion, ASTM Philadelphia, 1987.

18 M.E. Indig, J.E. Weber, *Corrosion '83*, paper #124, NACE, Houston, April, 1983.

19 W.R. Kassen, R.P. Jones, J.L Tollefson, *Corrosion '92*, paper #112, NACE, Houston, April, 1992.

20 M. Fox, *Corrosion '83*, paper #121, NACE, Houston, April, 1983.

21 C.C. Lin, R.L. Cowan, R.S. Pathania, *Corrosion '93*, paper #619, NACE, Houston, April, 1993.

22 L.G. Ljungberg, D. Cubicciotti, M. Trolle, *Corrosion '85*, paper #100, NACE, Houston, March, 1985.

23 M.J. Fox, "A Review of Boiling Water Reactor Chemistry:Science Technology, and Performance", NTIS Report# NUREG/CR-5115 ANL-88-42, February, 1989.

24 Y.J. Kim, *Corrosion '96*, paper #102, NACE, Houston, March, 1996.

25 R.S. Lillard, D.P. Butt, "Preliminary Spallation Neutron Source Corrosion Experiments: Corrosion Rates of Engineering Materials in a Water Degrader Cooling Loop Irradiated by an 800 MeV Proton Beam", LA-UR/LA-CP 96-1011, January, 1996.

26 J.R. Macdonald, Impedance Spectroscopy, Wiley Publishing, New York, 1987.

27 I. Epelboin, C. Gabrielli, M. Keddam, H. Takenouti, "Alternating-Current Impedance Measurements and Corrosion Rate Determination", in Electrochemical Corrosion Testing, ASTM STP 727, F. Mansfeld & U. Bertocci eds., ASTM, Ohio, pg. 150-66, 1981.

28 D.D. MacDonald, M.C.H. Mckubre, "Electrochemical Impedance Techniques in Corrosion Science" in Electrochemical Corrosion Testing, ASTM STP 727, F. Mansfeld & U. Bertocci eds., ASTM, Ohio, pg. 110-59, 1981

29 J.E.B. Randles, **Discussion of the Faraday Society**, vol. 1, no. 1, pp. 11-19, 1947.